Experimental Evaluation of UWB Ranging Performance for Correlation and ED Receivers in Indoor Environments

Chi Xu, and Choi. L. Law
Positioning & Wireless Technology Centre
Department of EEE, Nanyang Technological University
xuchi@ntu.edu.sg, ecllaw@ntu.edu.sg

Abstract

UWB signal reception in a ranging system can be accomplished by either coherent receiver or non-coherent receiver. Correlation receiver is a type of coherent receiver while energy detection (ED) receiver falls into the non-coherent category. In this paper, we evaluate their ranging performances using the channel profiles measured in various indoor environments. The effects of important system parameters such as sampling rate and threshold on the ranging performance are also investigated. Results show that ranging accuracy is heavily dependent on the system parameters settings, especially in LOS environment. The correlation receiver requires much higher sampling rate to achieve the same ranging accuracy as compared to ED receiver. The study also shows that regardless of receiver type used, the resultant ranging error for NLOS environments can be described by a unified model. The proposed model is validated by measurement data.

1. Introduction

The traditional geolocation systems such as Loran C and global positioning system (GPS) have been proven to be very effective in open space environment [1], [2]. These systems encounter difficulty to achieve satisfactory performance in dense multipath environment such as metropolis. The localization service in cities can be provided by existing mobile network and the accuracy has been proven to be reasonable for some applications [3]. When the localization scenario moves to indoor environments, the aforementioned systems fail due to multipath impairments and/or incapability of penetrating the building material. The indoor wireless network employing narrow band signal can realize indoor localization but its accuracy is limited by multipath fading [4].

Recently, ultra wideband (UWB) radio applied to sensor networks emerges as a viable solution for indoor localization applications [5], [6]. UWB radio has relative bandwidth larger than 20% or absolute bandwidth of more than 500 MHz. Such wide bandwidth greatly improves the multiple paths resolvability and hence alleviates the effects of multipath fading especially on the direct path [7]. Furthermore, spreading information over the large bandwidth reduces interference to other systems and lowers the probability of interception. Thus UWB signaling is especially suitable for indoor environments. It has been experimentally proved that UWB signal with time-of-arrival (TOA) estimation is able to provide high ranging accuracy with low-power and low-cost implementation [8].

Both correlation and energy detection (ED) receivers can be used for the reception of UWB signal in a ranging system. Correlation receiver demodulates the signal by correlating it with a well-designed template pre-stored or locally generated by the receiver [9]. To retain the fidelity of signal waveform, the sampling rate for correlation receiver should be at least

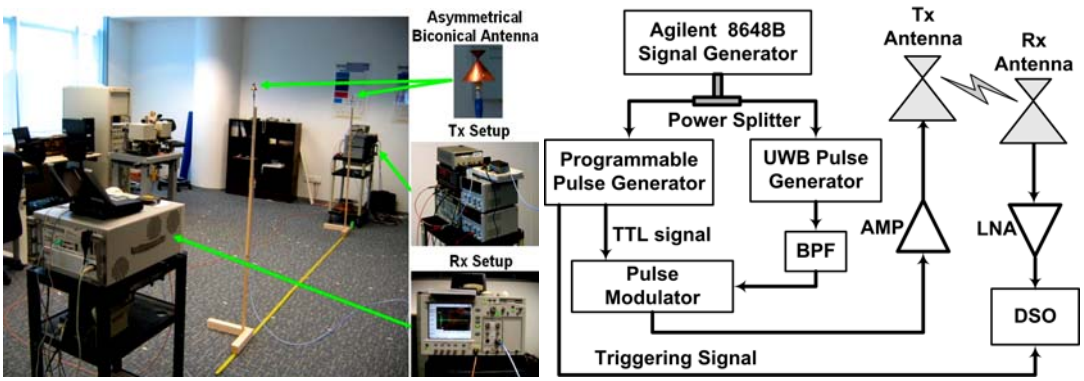

Figure 1. Measurement System: (a). Measurement Setup; (b). Block diagram.

Nyquist rate. It is well known that correlation receiver is optimal over AWGN channel since it maximizes the SNR of the received signal. However, such optimality is no longer assured in the indoor channel since the waveform shape of the direct path may be corrupted by the adjacent multipath components and/or be distorted when it penetrates the blockages such as walls. The Cramer-rao lower bound (CRLB) of the TOA estimation with correlation receiver in AWGN is given by [10]

$$\sigma_{toa}^2 \geq \frac{1}{2E_s\mathcal{A}/N_0} \tag{1}$$

where σ_{toa}^2 is the variance of TOA estimation, E_s is the energy of the ranging signal, $\mathcal{A}$ is the mean square bandwidth of the signal and N_0 is one-sided power spectral density. Therefore the ranging performance of correlation receiver can be improved by increasing SNR or signal bandwidth.

In contrast to the correlation receiver, ED receiver does not require the knowledge of the received waveform shape and thereby is more robust against signal waveform distortion. The sampling rate requirement of ED receiver is much lower than that of coherent receiver. Due to sampling granularity, the mean square error (MSE) of TOA estimation with ED receiver in AWGN is lower bounded by $T^2/12$ where T is the integration time interval (can also be interpreted as the sampling period) regardless of the signal bandwidth as SNR goes to infinity [11].

The ranging performance may be evaluated by either simulation or experiment. The performance comparison of correlation and ED receivers has been investigated by simulations using IEEE802.15.4a statistical channel model in [12]. However, the statistical channel model dose not capture the pulse distortion of individual path and simplifies some other aspects of the channel properties to lower down the implementation complexity. To gain the insight of how the receivers behave in a real propagation environment, we resort to the experimental approach.

In this paper, we consider the receivers employing threshold-based TOA estimation technique coupled with the first path detection strategy [13], [14]. The performance of correlation and ED receivers are evaluated and compared in different types of indoor

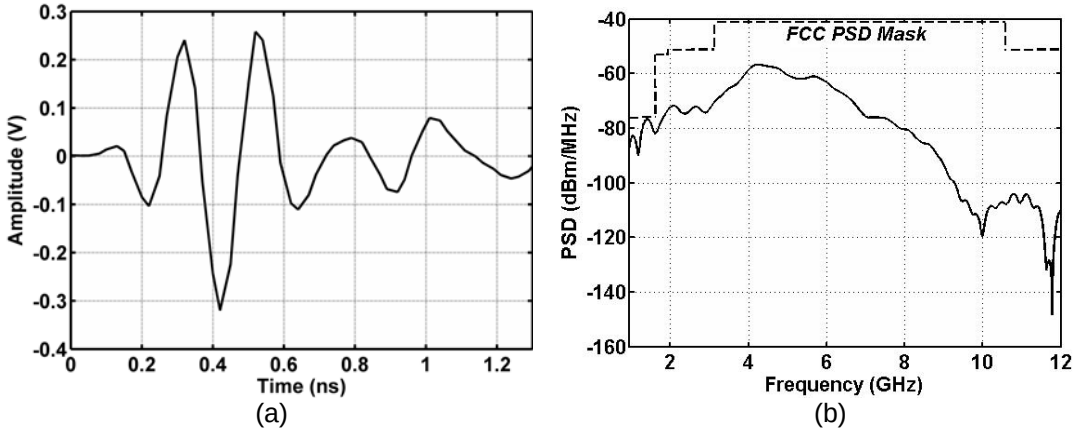

Figure 2. Pulse characteristic of the measurement system: (a). Received monocycle at D = 2 m; (b). The PSD of the transmitting pulse (Including transmitting antenna gain).

environments. The effects of important ranging parameters on the system performance are analyzed with the measured channel responses in the office environment. Finally, the ranging errors of both types of receivers in the NLOS scenario are characterized and modeled.

Section 2 describes the measurement setup and the measurement environments. The signal model and the post processing used to extract TOA information are discussed in Section 3. Section 4 presents the numerical results of the ranging performance for correlation and ED receivers. A unified ranging error model is developed in Section 5. Finally, the conclusion is drawn in Section 6.

2. Measurement description

The measurement setup and its block diagram are depicted in Figure 1. Agilent 8648B signal generator provides the clock for the entire measurement system. The kernel of the measurement setup is an in-house designed pulse generator generating UWB signal at a pulse repetition frequency (PRF) of 25 MHz [15]. A bandpass filter (BPF) is then used to shape the spectrum of the UWB signal. The PRF of the UWB signal is lowered down to 2 MHz by HP11720 pulse modulator whose TTL control signal is provided by Tabor 8600 programmable pulse generator. The resultant UWB signal consists of repetitive monocycles evenly distributed with time interval 500 ns which is sufficient long to avoid inter-symbol interference (ISI) caused by multipath. Tabor 8600 also provides a periodic rectangular waveform with period 500ns to the receiver via a low loss coaxial cable. This signal acts as triggering signal for the sampling process. The received UWB signal is amplified by low noise amplifier (LNA) before being sampled by the Agilent 86100B digital sampling oscilloscope (DSO). Both transmitting and receiving antennas are asymmetrical biconical antennas with omni-directional patterns [16]. Each antenna has approximately 2dBi gain in azimuth plane and is placed at 1.65 m above the floor. Every stored channel profile is the averaging of 512 channel snapshots and is of duration 400ns. Figure 2 (a) depicts that time domain waveform of the monocycle received at Tx-Rx distance D = 2 m. Figure 2 (b) shows that the power spectral density (PSD) of the transmitting pulse is compliant with the FCC PSD mask for indoor application [17]. Hence, our study reflects the performance of a ranging

Figure 3. Four measurement environments: office (upper left), laboratory room (upper right), open hall (lower left), and corridor (lower right).

system with realistic power constraint. Figure 3 shows four measurement environments among which the office environment is the most complicated environment having both line-of-sight (LOS) and non-line-of-sight (NLOS) scenarios. The office measurements were performed at the Positioning and Wireless Technology Center (PWTC) which is located at the 4th floor of Research Techno Plaza in the campus of Nanyang Technological University, Singapore. PWTC is a typical modern office with width 27.3 m, length 27.3 m and height 2.8 m. Its main area is soft partitioned and furnished with cupboards, metal cabinets, tables made of chipboard, plastic chairs, computers, etc. The main area is connected to other rooms directly or via very short corridors. Most of the walls inside the center are multilayer plasterboards. The external concrete wall of the center and the inner concrete walls surrounding the stair cases and elevators cause great attenuation to the signal. The detail layout of PWTC may be referred to [18]. Besides the indoor office, the rest of measurement environments are the laboratory room, open hall and corridor. Theses three environments are LOS scenarios. The laboratory room is a single room with some tables and measurement instruments placed by the walls. The door of the room is closed during measurement. Open hall is a large indoor open space where multipaths are mainly caused by floor, walls and some support beams. Corridor is a typical waveguide-like environment. Figure 4 shows the received channel profiles of different environments. The office and the laboratory environments are featured by dense multipath while the multipath of open hall and corridor are relatively sparse. In the NLOS scenario shown in Figure 4, the direct path in NLOS may be severely attenuated and thereby may be too weak to be detected. It is observed that the noise level varies spatially as well as temporally and the variation of noise power can be as much as 10 dB among the measured profiles due to the interference signals from other systems. In addition, the received signal level also varies spatially due to the variation of channel condition as the receiver position varies. Hence the measurement environments should be generally treated as dynamic environments.

During the measurement, the transmitter location was fixed and the receiver was placed at the spatial sample points uniformly distributed along some linear routes. The spacing between

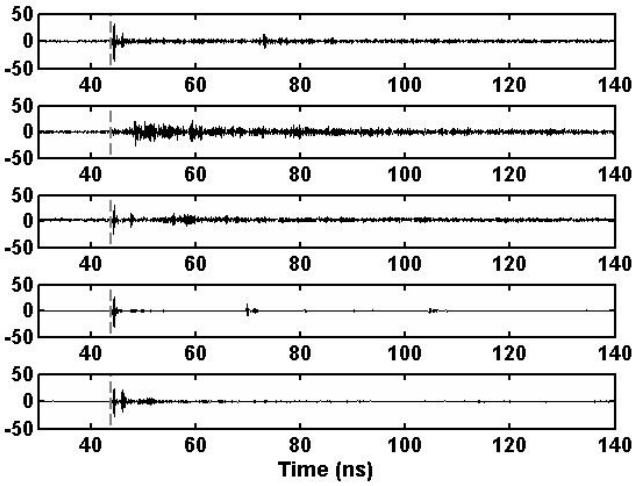

Figure 4. Received channel profiles at D = 5m in indoor office LOS, office NLOS, laboratory, open hall and corridor environments. The vertical scale is in milivolts. Vertical grey line in each plot shows the true TOA of the direct path signal.

any two adjacent points is 0.5 m for open hall, 1 m for corridor and 0.2 m for office and lab. Note that the spacing was chosen to be much larger than half wavelength to ensure independent sampling. For each measurement, both the transmitter (Tx) and the receiver (Rx) were kept stationary. The exact Tx-Rx distance is physically measured and recorded. The effective sampling rate of the oscilloscope is 40.5 GHz which is much higher than the Nyquist rate of the signal. The measurement system is calibrated prior to the measurements in order to obtain the pulse template and system delay.

3. TOA estimation with correlation and ED receivers

The measurement system can be viewed as a single user UWB system with a repetitive coder described in [19]. The local clocks of the transmitter and the receiver are aligned and hence one way ranging (OWR) can be performed [20]. The transmitter emits a signal at timing $t = t_{sta}$. After pre-filtering and averaging, the waveform of the received signal can be expressed as a supposition of the distorted and delayed replicas of the transmitted signal

$$r(t) = \sqrt{E_{tx}} \sum_{l=0}^{N_{mul}-1} \alpha_l \xi_l p_l \left(t - \tau_l - t_{toa}\right) + n(t) \tag{2}$$

where $\sqrt{E_{tx}}$ is the energy of the transmitting pulse, N_{mul} is the number of multipath, $p_l(t)$ is the energy-normalized monocycle of the l^{th} path, α_l , ξ_l and τ_l are the path gain, path polarity and relative propagation delay of the l^{th} path, $t_{toa} = \tau_d + \tau_{sys} + t_{sta}$ is the true TOA, τ_d is the absolute propagation delay of the direct path, τ_{sys} is the delay introduced by system hardware, and $n(t)$ is the noise process. $r(t)$ is the raw waveform that will be further processed by different algorithms to estimate TOA.

For correlation receiver, $r(t)$ is first cross-correlated with the pulse template $p_{tm}(t)$ which has unit energy and finite time support on $[0, T_{tm}]$. The template is obtained by extracting the direct path from the LOS waveform measured at D = 2 m with a proper windowing function. Since the pulse template $p_{tm}(t)$ has very high SNR, it can be considered as quasi-noise free. The cross-correlation between the template and the received signal is given by

$$r_c(t) = \int r(\xi) p_{tm}(\xi - t)\, d\xi . \tag{3}$$

Then the CLEAN algorithm is performed on $r_c(t)$ to estimate the multipath amplitude and arrival timings. The CLEAN algorithm was first introduced in [21] and has been widely used in the radio astronomy and microwave communities. It was applied to UWB channel estimation in [22]. A variant of the CLEAN algorithm introduced in [23] are herein employed to extract path information. Suppose that the channel estimation using CLEAN gives a vector of path amplitude $\mathbf{x} = [x_0, x_1, ..., x_{M-1}]$ with respected to the delay $\mathbf{t} = [t_0, t_1, ..., t_{M-1}]$ which has been sorted according to the ascending order.

For ED receiver, $r(t)$ passes through a square law device followed by a finite time integrator. Starting from timing t_{sta}, the integrator successively integrates the output of the square law device with time interval T. The sampling rate of ED receiver is $1/T$. The sample vector is denoted as $\mathbf{z} = [z_0, z_1, ..., z_{N-1}]$ with the k[th] sample given by

$$z_k = \int_{t_{sta}}^{t_{sta}+kT} |r(t)|^2 \, dt, k = 0,1,...,N-1 . \tag{4}$$

To fairly compare with the correlation receiver, the samples are converted to $x_k = \sqrt{z_k / T}\ \forall k = 0,1,...,N-1$ which is associated with timing $t_k = (k + 1/2)T + t_{sta}$.

With the amplitude vector $\mathbf{x}$ of correlation or ED receiver, we take the first path crossing a predefined threshold as the direct path and estimate its arrival time as TOA of the signal. Let the largest sample be $x_{\max}$ associated with timing $t_{\max}$. The estimated TOA is

$$\hat{t}_{toa} = \left(\arg\min_k [x_k > \gamma] + 1/2\right) T + t_{sta}, t_{\max} - \delta \le t_k \le t_{\max} \tag{5}$$

where γ is the detection threshold and δ is the searching duration. To reduce the false alarm triggered by the noise samples, we propose the following empirical setting strategy making use of the information of received signal strength and noise statistics:

$$\gamma = \begin{cases} \max\left[\beta x_{\max}, \xi_{floor}\right], & if\ \xi_{floor} \le x_{\max} \\ x_{\max}, & if\ \xi_{floor} > x_{\max} \end{cases} \tag{6}$$

where $\xi_{floor} = \mu_{noise} + m\sigma_{noise}$ represents a threshold level proportional to the noise floor, μ_{noise} and σ_{noise} are the mean and standard deviation of noise only samples, m and β are positive real numbers and $0 \le \beta < 1$. For correlation receiver, μ_{noise} and σ_{noise} are the mean and standard deviation of $n(t)$. For ED receiver, μ_{noise} and σ_{noise} are the mean and standard deviation of the noise-only energy samples. When SNR is low, $\beta x_{\max}$ is small and the threshold is likely to be set by ξ_{floor} which prevents the estimation from falling into noise only region prior to the direct path. When SNR increases, the threshold becomes dominated by $\beta x_{\max}$ which rises with increasing SNR and hence the false alarm rate is reduced. Therefore this setting strategy ensures that the false alarm rate has a ceiling regardless of SNR and decreases with increasing SNR. For the following numerical

Table 1. Performance of correlation and ED receivers in different environments.

Environment	Number of profiles	Maximum measurement distance (m)	Correlation with sampling rate 40.5 GHz		ED with sampling rate 1 GHz	
			RMSE (m)	MAE (m)	RMSE (m)	MAE (m)
Office LOS	326	26	0.023	0.018	0.101	0.084
Office NLOS	977	26	4.800	2.261	5.504	2.650
Laboratory	271	5	0.084	0.031	0.172	0.132
Open Hall	61	30	0.021	0.017	0.100	0.084
Corridor	31	30	0.019	0.015	0.102	0.085

study, we set m=15dB=5.6234. Note that $\hat{t}_{toa}$ includes the delay introduced by hardware as well as propagation delay. To calibrate out the unknown hardware delay τ_{sys}, we estimate the arrival time of signal captured in a LOS profile at a reference distance D_{ref} which is chosen as 2 m. Denote the true arrival time of the direct path in the reference profile as t_{ref} and its estimated version as $\hat{t}_{ref}$. Since the captured reference profile can be considered as quasi noise free due to the high SNR condition, $\hat{t}_{ref}$ may be approximated as t_{ref} which subsumes the same hardware delay as t_{toa}. The one way distance is then estimated as $\widehat{D} = c\left(\hat{t}_{toa} - \hat{t}_{ref}\right) + D_{ref}$ where c is velocity of light. The ranging error is defined as $\varepsilon = \widehat{D} - D$ where D is the true distance.

4. Performance comparison of correlation receiver and ED receiver

In this section, the performances of correlation and ED receivers are compared using measured profiles and algorithms described in Section 3, following by which the effects of system parameters on the ranging performance are investigated. Both root mean square error (RMSE) and mean absolute error (MAE) are used as ranging performance criteria [11], [24]. RMSE and MAE are defined as

$$RMSE = \sqrt{E\left[\varepsilon_i^2\right]} = \sqrt{\sum_{i=0}^{N_{tot}-1}\left(\varepsilon_i^2 / N_{tot}\right)} \quad , \tag{7}$$

$$MAE = E\left[\left|\varepsilon_i\right|\right] = \sum_{i=0}^{N_{tot}-1}\left|\varepsilon_i / N_{tot}\right| \tag{8}$$

where N_{tot} is the total number of measured profiles used to generate the RMSE and ε_i is the ranging error of the i[th] profile. With the Cauchy's inequality (see 3.2.9 in [25]), it is readily show that

$$\frac{1}{N_{tot}}\left(\left|\varepsilon_0\right| + \left|\varepsilon_1\right| + ... + \left|\varepsilon_{N_{tot}-1}\right|\right)^2 \le \left(\varepsilon_0^2 + \varepsilon_1^2 + ..., \varepsilon_{N_{tot}-1}^2\right). \tag{9}$$

Eqn. (9) indicates $MAE \le RMSE$. Hence with the same set of $\{\varepsilon_i\}$, MAE is always smaller than RMSE.

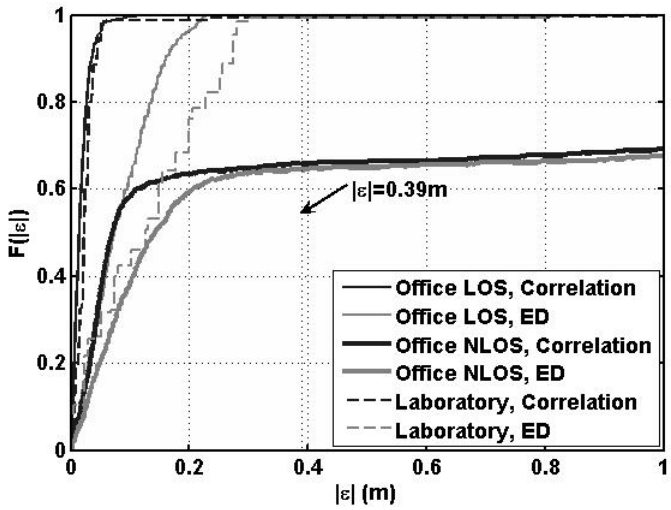

Figure 5. CDF of ranging errors with β = 0.2, δ = 50 ns and T = 1 ns.

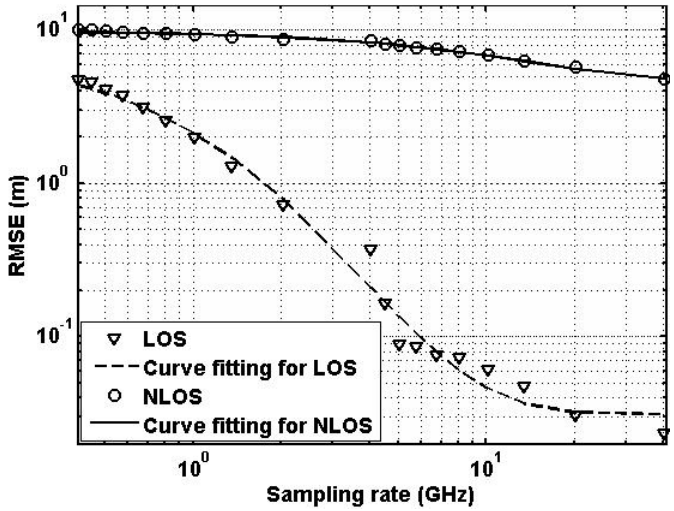

Figure 6. RMSE versus sampling rate for correlation receiver in the office environment with β = 0.2, and δ = 50 ns.

Table 1 shows the ranging performance evaluated with β = 0.2, T = 1 ns and δ = 50 ns for different environments. Both ED and correlation receivers are able to achieve centimeter accuracy in LOS scenarios regardless of type of environments. The estimated ranging performance of office NLOS is much worse than that of LOS environments. This is attributed to the blockages that may attenuate, distort and delay the direct path.

Figure 5 shows the cumulative distribution functions (CDFs) $F(|\varepsilon|)$ of ranging errors with correlation and ED receivers. Since the width of the UWB monocycle used in this measurement is approximately 1.3 ns corresponding to an electrical length 0.39 m, we may

declare the occurrence of an incorrect detection of direct path when $|\varepsilon| > 0.39$ m. The correct detection probability $P(|\varepsilon| \leq 0.39$ m) of both correlation and ED receivers in the LOS scenarios are very close to 1. In NLOS, the probability of both correlation and ED receivers are only approximately 0.66. Within the interval $|\varepsilon| \in [0$ m, 0.39 m], for the same type of environment, the CDF curves of correlation receiver lies above those of ED receiver due to the fact that correlation receiver has higher time resolution than ED receiver.

The results in Table 1 and Figure 5 do not lead to the immediate conclusion that correlation receiver always outperforms ED receiver since those results are computed with certain system parameter settings. When the settings such as sampling rate are changed, the correlation receiver may have worse performance as we should show in the following discussion.

The performance of correlation receiver is heavily dependent on the sampling rate. In the experiment, captured waveform is oversampled by the oscilloscope with sampling rate 40.5 GHz which is much higher than the Nyquist rate. To investigate the effect of sampling rate on correlation receiver, $r(t)$ and $p_{tm}(t)$ are downsampled by keeping every q^{th} sampling starting with the first sample. We consider q = {1,2,…,8,9,10,20,…,90,100}. The signal frequency band of the UWB pulse used in the measurement is approximately [3.5 GHz, 6.4 GHz] if cutoff frequencies are defined as the frequencies where the power is -10 dB lower than the peak power in PSD plot. Hence with sampling rate f_s = 40.5/q GHz, $\forall q \geq 4$, the waveform is undersampled. Under-sampling induces the distortion on the pulse shape of the template as well as the received signal. When the sampling is too low ($q \geq 30$), the pulse template becomes a delta function due to its finite time support. Figure 6 depicts the RMSE in office LOS environment as the sampling rate f_s varies. It is observed that the performance deteriorates as the sampling rate decreases. The reason is that decreasing of sampling rate makes the pulse distortion more severe and hence the correlation operation captures less energy of the direct path. In addition, lower sampling rate also reduces the time solution of the system and thereby reduces the path resolvability of the ranging algorithm. Note that for ED receiver, the sample rate is $1/T$. If sampling rate is 1 GHz, RMSE of the correlation receiver is 1.985 m in LOS which is much worse than that of ED receiver which is only 0.101m as shown in Table 1.

The relationship between RMSE and sampling rate for a correlation receiver as shown in Figure 6 can be modeled as

$$RMSE = 10^{(b_0 \exp(b_1 f_s) + b_2)} . \quad (10)$$

The sampling rate in the above model has the unit of GHz. The model coefficients are obtained by curve fittings. For LOS, the coefficients are $b_0 = 2.386, b_1 = -0.262$ and $b_2 = -1.503$. For NLOS, the coefficients are $b_0 = 0.336, b_1 = -0.066$ and $b_2 = 0.662$.

Figure 7 shows the relationship between RMSE and integration time of ED receiver for office environment. In the LOS case, RMSE monotonically increases with integration time due to decreasing time solution of the system. In NLOS, surprisingly, RMSE improves with larger T within [0 ns, 5 ns]. A possible explanation for this counter-intuitive observation is given as follows. Longer integration time means the energy sample is expected to be larger. Such accumulative effect benefits more on the samples with smaller relative delays since earlier incoming paths are statistically stronger than the later incoming paths. Hence the probability of detecting the earlier incoming paths increases. Note that earlier incoming paths

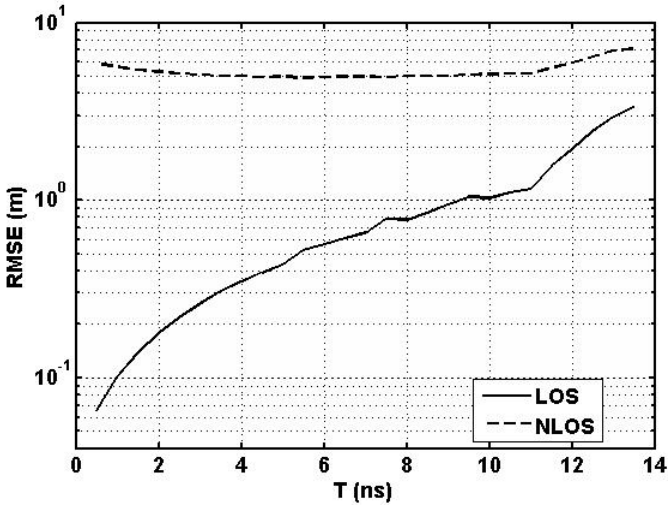

Figure 7. RMSE versus integration time for ED receiver in the office environment with β = 0.2 and δ = 50 ns.

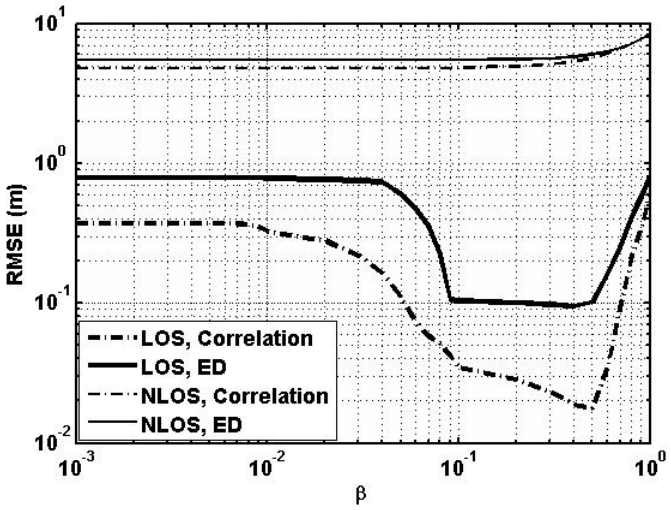

Figure 8. RMSE versus β in the office environment with δ = 50 ns and T = 1 ns.

are closer to the direct path. When this accumulative effect has heavier impact on the ranging accuracy than the degradation effects caused by the reduced time resolution, the performance improves. At T = 5 ns, RMSE curve hits a floor and remains unchanged until the integration time increases to T = 11ns beyond which the curve goes up again due to the domination of reduced time resolution effect on the ranging accuracy.

Figure 8 depicts the ranging performance as β varies. When β is small, the performance is almost invariable. The reason is that according to threshold setting strategy in (6), when $\beta Y_{\max}$ is too small, the threshold is determined by the

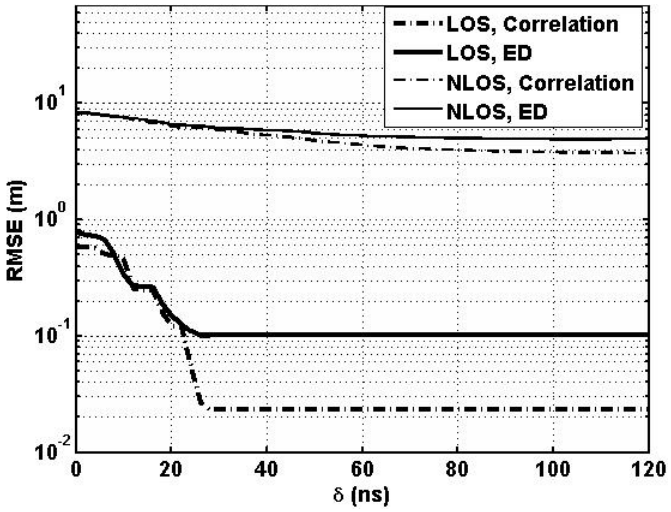

Figure 9. RMSE versus δ for ED receiver in the office environment with β = 0.2 and T = 1 ns.

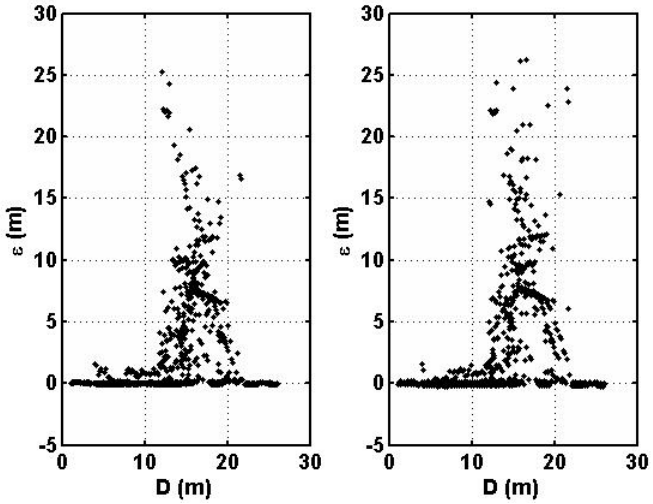

Figure 10. Scatter plot of ranging errors in NLOS environment: (a). correlation receiver. (b). ED receiver with parameter settings β =0.2, δ =50ns, and T=1ns.

parameter m which is unchanged. As β increases, RMSE in LOS decreases first and then increases again. In NLOS, RMSE monotonically increases with the increasing of β. When β = 1, the largest resolved path is adopted as direct path. Note that in both LOS and NLOS scenarios β = 1 is not the optimum threshold setting since the direct path may not be the strongest path even in LOS. The adjacent multipaths may constructively overlap with each other to create a path stronger than the direct path. In addition, the direct path may destructively overlap with the following multipath. It is also observed that the ranging accuracy is less sensitive to the threshold variation in NLOS than in LOS.

Figure 9 shows the impact of observation window length on the ranging performance. In both LOS and NLOS, increasing the window length lowers the probability of missing the direct path while increases false alarm rate. Since the threshold setting strategy in Eqn. (6) effectively prevents the occurrence of false alarm event, RMSE is monotonically decreased with increasing of window length. When the window length is widened beyond a transition point which is about δ = 30 ns for LOS and δ = 100 ns for NLOS, the performance reaches the saturation region. Generally, NLOS requires a wider observation window since the probability that the direct path is further apart from the strongest path is higher in NLOS than in LOS.

5. Ranging error characterization and modeling

Ranging error model can be used to simulate the performance of ranging system or provide statistics to the positioning or tracking algorithm [26]. There are two methods to model the ranging error in NLOS environment. The first approach is to model the ranging error as combinations of some random variables with each assigned explicit physical meaning [27]. The second approach is to model the probability density function (PDF) of the ranging errors. In [26] and [28], the PDF of the normalized ranging errors in NLOS are modeled as a mixture of Gaussian distribution and exponential distribution. The parameters in the mixture distribution are assumed to be distance independent. Here we use the second method. Unlike the model in [26] and [28], we model the PDF of the ranging error but not the normalized ranging error as a mixture distribution with the parameters being distance dependent. The motivation is to bypass the normalization process and explicitly relate the model coefficients to the distance D .

Figure 10 shows the scatter plot of the ranging error ε in office NLOS environment. For both the correlation and ED receivers, the mean and variance of the ranging error ε increase as D increases. The absence of negative errors with large absolute values implies that the false alarm rate is negligible due to the threshold setting strategy in Eqn. (6). Thus the channel is the main source causing large errors. The PDF of ε for a particular distance D is given by

$$f(\varepsilon;D) = \big(1-W(D)\big)\frac{1}{\sigma_G\sqrt{2\pi}}e^{-\frac{\varepsilon^2}{2\sigma_G^2}} + \frac{\varepsilon+|\varepsilon|}{2}W(D)\lambda(D)e^{-\lambda(D)\varepsilon} \tag{11}$$

where $W(D)$ is a distance-dependent weighting factor, σ_G is the standard deviation of Gaussian distribution, and $\lambda(D)$ is the distance-dependent parameter for exponential distribution. σ_G is assumed to be independent of distance. The Gaussian distribution accounts for the effects of measurement noise and the exponential distribution is related to the impact of channel effects.

The mixture distribution with PDF expressed in (11) has mean

$$\mu = \frac{W(D)}{\lambda(D)} \tag{12}$$

and variance

$$\sigma^2 = \big(1-W(D)\big)\sigma_G^2 - \left(\frac{W(D)}{\lambda(D)}\right)^2 + \frac{2W(D)}{\lambda^2(D)} \ . \tag{13}$$

By solving (12) and (13) , we have

$$\lambda(D) = \frac{-\left(\mu^2 + \sigma^2 - \sigma_G^2\right) + \sqrt{\left(\mu^2 + \sigma^2 - \sigma_G^2\right)^2 + 8\mu^2\sigma_G^2}}{2\mu\sigma_G^2} . \quad (14)$$

Substituting (14) into (12), $W(D)$ is computed as

$$W(D) = \frac{-\left(\mu^2 + \sigma^2 - \sigma_G^2\right) + \sqrt{\left(\mu^2 + \sigma^2 - \sigma_G^2\right)^2 + 8\mu^2\sigma_G^2}}{2\sigma_G^2} . \quad (15)$$

To estimate σ_G, we form a data set S_{neg} containing only the negative errors. Assume that the information of the Gaussian distribution can be fully obtained by exploiting the statistical property of the elements in S_{neg}. Using the symmetry property of Gaussian distribution, a new data set S_{sym} is constructed with the elements from S_{neg} and the inverse of them. The total number of points in S_{sym} is denoted by N_G. Denote the mean of the elements in S_{sym} as μ_G. Due to the symmetry property of those elements, $\mu_G = 0$. σ_G is then estimated as the variance of the elements in S_{sym}:

$$\sigma_G = \sqrt{\frac{1}{N_G - 1}\sum_i \left(\varepsilon_i - \mu_G\right)^2}, \varepsilon_i \in S_{sym} . \quad (16)$$

An intuitive way to obtain $W(D)$ and $\lambda(D)$ is to estimate their function values from a large number of channel realizations for D. However, this method is impractical since the number of channel profiles associated with the same distance D is usually too few to generate statistics. To overcome this problem, we propose a low-complexity method to estimate $W(D)$ and $\lambda(D)$. First, the set of true distance $\{D_i\}$ are sorted and divided into six subsets $\mathcal{B}_j, j = 1,...,6$ which are defined by $\mathcal{B}_1 = \{D_i \le 5m\}$, $\mathcal{B}_2 = \{5 \le D_i \le 7.5m\}$, $\mathcal{B}_3 = \{7.5 \le D_i \le 10m\}$, $\mathcal{B}_4 = \{10 \le D_i \le 12.5m\}$, $\mathcal{B}_5 = \{12.5 \le D_i \le 15m\}$, $\mathcal{B}_6 = \{15 \le D_i \le 17.5m\}$. This is indeed a quantization process of distance axis. Every subset contains sufficient number of profiles (≥ 80) to generate statistics. Each subset is associated with the a mean distance calculated by

$$D_{mean\_j} = \sum_i D_i, D_i \in \mathcal{B}_j . \quad (17)$$

For each subset, its variance σ_j^2 and mean μ_j are then calculated from the ranging errors associated with the distance values in that subset. As shown in Figure 11 and 12, the relationship between λ or W versus physical distance D for both correlation and ED receivers can be modeled as

$$\lambda(D) = B_1 / \left(\exp\left(B_2 D\right) + B_3\right), \quad (18)$$

and

$$W(D) = 1 / \left(C_1 \exp\left(-C_2 D\right) + 1\right). \quad (19)$$

As D increases, the direct path strength decreases due to longer traveling distance and more obstructions along the direct path. The probability that the multipath is detected as the

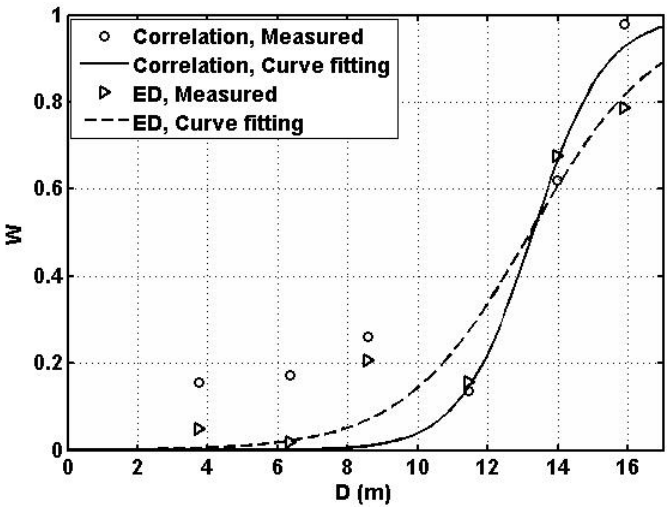

Figure 11. Curve fitting for W.

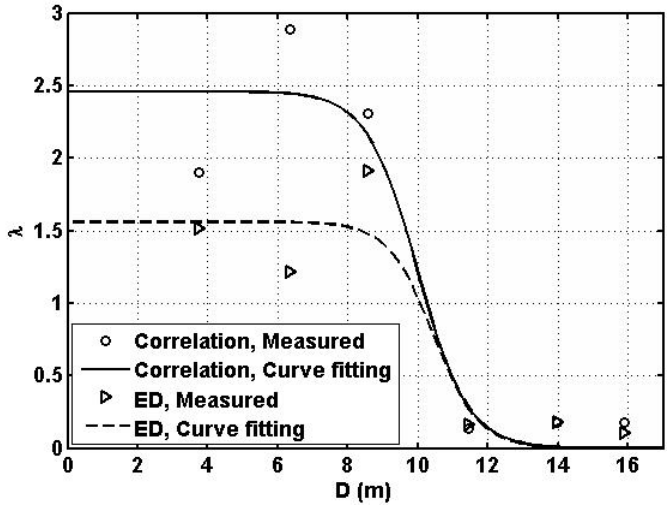

Figure 12. Curve fitting for λ.

direct path is increased and hence W increases. Moreover, as distance increases, the chance that the earlier arrival paths are blocked or severely attenuated are increased, and hence it is more likely that the multipath with larger relative delay is detected as the direct path is also increases. This phenomenon is explained by the decreasing of λ. By curve fitting, the coarse estimation of the parameters in (18) and (19) may be obtained. Due to the quantization of distance axis, the estimated model parameters are not very accurate. Hence, the fine estimation of the parameters is obtained by tuning the parameters to minimize the difference between the empirical CDF function (generated from empirical ranging error set $\{\varepsilon_i\}, 0 \le i \le N_{tot} - 1$) and the following model based CDF function

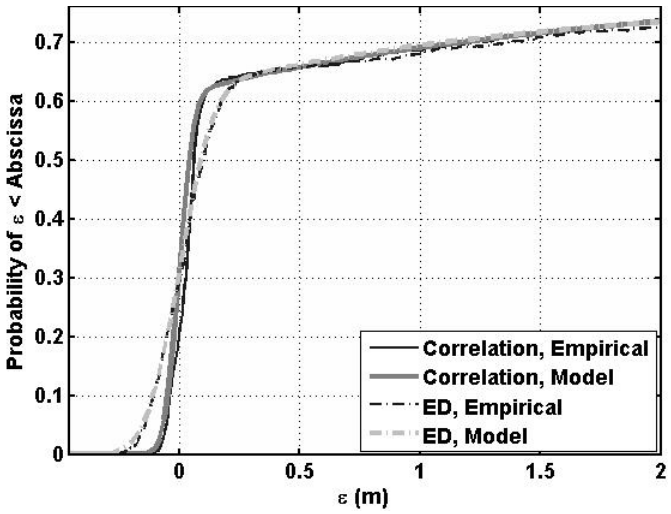

Figure 13. Comparison of CDFs generated from measurement data and the proposed model.

Table 2. Fitting Coefficients

	B_1	B_2	B_3	C_1	C_2
Correlation	2.459×10^6	1.358	9.994×10^5	3.915×10^5	0.9701
ED	1.559×10^7	1.544	9.986×10^6	1.152×10^3	0.5544

$$F(\varepsilon) = \frac{1}{N_{tot}} \sum_{i=0}^{N_{tot}-1} F(\varepsilon; D_i) \tag{20}$$

where $F(\varepsilon; D_i) = \int_{-\infty}^{\varepsilon} f(\xi; D_i) d\xi$. Figure 13 indicates the close match between the two functions after fine tuning of the parameters. The final estimated parameters for correlation and ED receivers are given in Table 2.

6. Conclusion

In this paper, the ranging performance of correlation and ED receivers are evaluated and compared based on measured channel responses captured in the indoor environments. The results show that ranging performances of correlation and ED receivers are heavily dependent on the system parameters setting, especially in LOS environment. The correlation receiver outperforms ED receiver only if the sampling rate of correlation receiver is much higher that that of ED receiver. It is also found that the ranging error model of both types of receivers can be described by a unified model with distance-dependent parameters.

References

[1] Owen Wilkes and Nils Petter Gleditsh, *Loran-C and Omega*, Norwegian University Press, 1987.

[2] B. W. Parkinson and J. J. Spiker Jr., *Global Positioning System: Theory and Applications*, American Institute of Aeronautics and Astronautics. Inc., 1996.

[3] J. J. Caffery, Jr. *Wireless Location in CDMA Cellular Radio Systems*, Kluwer Academic Publishers, 2000.

[4] A. M. Ladd, K. E. Bekris, A. Rudys, L. E. Kavraki, and D. S. Wallach, "On the feasibility of using wireless Ethernet for indoor localization," *IEEE Trans. Robot. Autom.* vol. 20, no. 3, pp. 555-559, June 2004.

[5] I. F. Akyildiz, W. Su, Y. Sankarasubramaniam, and E. Cayirci, "A survey on sensor Networks," *IEEE Commun. Mag.,* Aug. 2002, pp. 102-104.

[6] N. Patwari, Joshua N. Ash, S. Kyperountas, A. O. Hero III, R. L. Moses, and N. S. Correal, " Locating the nodes: cooperative localization in wireless sensor networks," *IEEE Signal Process. Mag.*, July 2005, pp. 54-69.

[7] M. Z. Win and R. A. Scholtz, "On the robustness of ultra-wide bandwidth signals in dense multipath environments," *IEEE Commun. Lett.,* vol.2, pp. 51-53, Feb. 1998.

[8] R. J. Fontana, "Experimental results from an ultra wideband precision geolocation system," *Kluwer Academic/Plenum Publishers,* 2000.

[9] M. Z. win and R. Scholtz, "Impulse radio: How it works," *IEEE Commun. Lett.*, vol.2, pp. 36-38, Feb. 1998.

[10] S. M. Kay, *Fundamentals of Statistical Signal Processing: Estimation Theory*, Upper Saddle River, NJ: Prentice-Hall, 1998.

[11] D. Dardari, C. -C. Chong, and M. Z. Win, "Analysis of threshold-based TOA estimation in UWB channels," in *Proc. Of European Signal Process. Conf. (EUSIPCO)*, Florence, Italy, Sep. 4, 2006.

[12] I. Guvenc and Z. Sahinoglu, and P. V. Orlik, "TOA estimation in IR-UWB systems with different transceiver types," *IEEE Trans. Microw. Theory Tech.*, vol. 54, no. 6, pp. 1876-1886, Jun. 2006.

[13] B. Denis, J. Keignart, and N. Daniele, "Impact of NLOS propagation upon ranging precision in UWB systems," in *Proc. IEEE Conf. Ultrawideband Syst. Technol.,* Reston, VA, Nov. 2003, pp. 379-383.

[14] I. Guvenc and Z. Sahinoglu, "Threshold-based TOA estimation for impulse radio UWB systems," in *Proc. IEEE Int. Conf. on UWB,* Zurich, Switzerland, 05-08 Sept. 2005, pp. 420-425.

[15] Z. N. Low, J. H. Cheong and C. L. Law, "Novel low cost higher derivative Gaussian pulse generator circuit," in *Proc. Int. Conf. on Commun. Syst. (ICCS2004),* Singapore, Sep 6-8, 2004, pp. 30-34.

[16] Kojj Nagasawa, and Isamu Matsuzuka, "Radio field consideration of biconical horn antenna with different flare angles," *IEEE Trans. On Antenna and Propagation*, vol. 36, no. 9, Sep., 1998.

[17] "First Report and Order 02-48," Federal Communications Commission, Washington, DC, 2002.

[18] Chi Xu and Choi. L. Law, "Experimental evaluation of UWB ranging performance for correlation and ED receivers in dense multipath environment," in *Proc. Future Generation Communication and Networking (FGCN2007)*, vol. 2, Jeju Island, Korea, 6-8 Dec. 2007, pp. 186-192,.

[19] M. G. Di Benedetto, and G. Giancola, *Understanding Ultra Wide Band Radio Fundamentals*, Prentice Hall PTR, NJ, 2004.

[20] B. Denis, "UWB localization techniques," IEEE 802.15 TG4a, Tech Rep. P802.15-04/418r0, Aug., 2004. [Online]. Available at http://www.ieee802.org/15/pub/2004/.

[21] J. A. Hogborm, "Aperture synthesis with a non-regular distribution of interferometer baselines," *Astron. And Astrophys. Suppl. Series*, vol. 15, pp. 417-426, 1974.

[22] J. M. Cramer, R. A. Scholtz, and M. Z. Win, "Evaluation of an ultra-wideband propagation channel," *IEEE Trans. Antennas Propag.,* vol. 50, no.5, May 2002, pp. 561-570.

[23] S. M. Yano, "Investigating the Ultra-wideband indoor wireless channel," in *Proc. IEEE Veh. Technol. Conf.*, vol. 3, pp. 1200-1204, Birmingham , Ala, USA, May 2002.

[24] I. Guvenc and Z. Sahinoglu, "Threshold selection for UWB TOA estimation based on Kurtosis analysis," *IEEE Commun. Lett.*, vol. 9, no.12, pp. 1025-1027, Dec. 2005.

[25] M. Abramowitz and I. A. Stegun, *Handbook of Mathematical Functions with Formulas, Graphs, and Mathematical Tables*, New York: Dover, 1970.

[26] B. Denis, J. B. Pierrot, and Chadi Abou-Rjeily, "Joint distributed synchronization and positioning in UWB Ad Hoc networking using TOA," *IEEE Trans. Microw. Theory Tech.*, vol. 54, pp.1896-1911, June 2006.

[27] B. Alavi and K. Pahlavan, "Modeling of the TOA-based distance measurement error using UWB indoor radio measurements," *IEEE Commun. Lett.* vol. 10, no. 4, April 2006.

[28] B. Alavi and K. Pahlavan, "Bandwidth effect on distance error modeling for indoor geolocation," in *Proc. IEEE PIMRC 2003,* Beijing, China, vol. 3, pp. 2198-2202, Sept. 2003.

Authors

Chi Xu is a Ph.D. student in electrical and electronic school of Nanyang Technical University, Singapore. His research interests include wireless communication, statistical signal processing for ranging and positioning applications and ultra wideband radio. He is a member of IEEE.

Dr. Choi Look Law received his BEng. and Ph.D. degree from King's College, London in 1983 and 1987 respectively. His research interests are in digital beam forming array antenna, ultra wideband microwave circuits, wideband channel characterization and modeling, radio frequency identification and wireless networking and positioning systems. He is a member of IEEE.

He is a co-founder of RFNET, a company that specializes in RF and wireless networking products and services.